

## Hydrodynamics of discrete-particle models of spherical colloids: A multiparticle collision dynamics simulation study

Simón Poblete,<sup>\*</sup> Adam Wysocki,<sup>†</sup> Gerhard Gompper,<sup>‡</sup> and Roland G. Winkler<sup>§</sup>

*Theoretical Soft Matter and Biophysics, Institute of Complex Systems and Institute for Advanced Simulation,  
Forschungszentrum Jülich, D-52425 Jülich, Germany*

(Received 24 June 2014; published 29 September 2014)

We investigate the hydrodynamic properties of a spherical colloid model, which is composed of a shell of point particles by hybrid mesoscale simulations, which combine molecular dynamics simulations for the sphere with the multiparticle collision dynamics approach for the fluid. Results are presented for the center-of-mass and angular velocity correlation functions. The simulation results are compared with theoretical results for a rigid colloid obtained as a solution of the Stokes equation with no-slip boundary conditions. Similarly, analytical results of a point-particle model are presented, which account for the finite size of the simulated system. The simulation results agree well with both approaches on appropriate time scales; specifically, the long-time correlations are quantitatively reproduced. Moreover, a procedure is proposed to obtain the infinite-system-size diffusion coefficient based on a combination of simulation results and analytical predictions. In addition, we present the velocity field in the vicinity of the colloid and demonstrate its close agreement with the theoretical prediction. Our studies show that a point-particle model of a sphere is very well suited to describe the hydrodynamic properties of spherical colloids, with a significantly reduced numerical effort.

DOI: [10.1103/PhysRevE.90.033314](https://doi.org/10.1103/PhysRevE.90.033314)

PACS number(s): 47.11.-j, 02.70.-c, 05.10.-a

### I. INTRODUCTION

Molecular simulation of soft matter systems typically involves a broad range of time and length scales, thus posing substantial computational challenges and rendering certain first-principle studies unfeasible. Coarse-grained approaches [1] are a common way to bridge and tackle such scale separations. A reduction in the number of degrees of freedom of a system allows for studies of larger systems and longer times at the expense of the details of the model. Therefore, the physical properties to be reproduced in a coarse-grained representation must be chosen carefully. Static properties such as structures [2,3], force on the coarse-grained sites [4–6], or certain thermodynamic properties [7] can be adjusted by designing a proper force field between the components of the new, simplified representation of the system. Transport properties, however, require a different treatment. Considering biological systems as an example, the aqueous environment plays a major role in their dynamical aspects and the fluid-mediated interactions need to be correctly captured. As a consequence, several mesoscale simulation techniques emerged in the past few decades, which bridge the time scales between the embedded entities and the fluid dynamics [8–12]. These mesoscale methods treat the fluid in a simplified way and ensure the conservation of momentum and mass and thus yield proper hydrodynamic behavior on large length scales [13]. Among them, the multiparticle collision dynamics (MPC) approach [10–12] is very well suited for simulations of soft matter systems. Multiparticle collision dynamics is a particle-based method, which naturally includes thermal fluctuations and can efficiently be coupled to embedded

particles whose dynamics is governed by Newton's equations of motion [11,12,14–16].

The properties of the MPC fluid itself have been studied intensively and are well understood by now [10–13,13,15,17–22]. Moreover, the equilibrium and nonequilibrium dynamical properties of a broad spectrum of soft matter systems embedded in the MPC fluid have been studied. Examples cover polymers in solution [14,23–28], colloids [29–36], proteins [37], vesicles [38], and red blood cells [39,40].

Colloids have been introduced as solid objects with slip [15,30,31,34,36] or no-slip (stick) [21,31,32,34] boundary conditions. Specifically, no-slip boundary conditions require considerable effort. Usually, the so-called bounceback rule is applied at the colloid surface [21,30,32], where velocities are reverted upon collision in a comoving reference frame [34]. This requires the calculation of the MPC particle's relative position and velocity with respect to a colloid and, in addition, phantom particles have to be taken into account [32]. Here a simpler model may be more efficient without appreciable deviation of physical properties.

In this paper we study the hydrodynamic properties of such a simplified model of a spherical colloid. The colloid is described as a spherical shell composed of point particles, which are connected by suitable elastic bonds to maintain its shape. Such an approach has already been proposed in Ref. [41] in combination with lattice Boltzmann simulations. Our simulations show that the translation and rotational velocity correlation functions agree very well with those of the solution of the Navier-Stokes equations for a solid colloid. Hence, our discrete-shell colloidal model is very well suited for simulations of colloidal particles. Our studies not only are useful for spherical colloids, but will also be valuable for extensions to other rigid structures such as cubes, sheets, platelets, and nonconvex and irregular bodies [42–44] embedded in a MPC fluid, which can be designed in a similar fashion or be built using these elements as building blocks.

<sup>\*</sup>s.poblete@fz-juelich.de

<sup>†</sup>a.wysocki@fz-juelich.de

<sup>‡</sup>g.gompper@fz-juelich.de

<sup>§</sup>r.winkler@fz-juelich.de

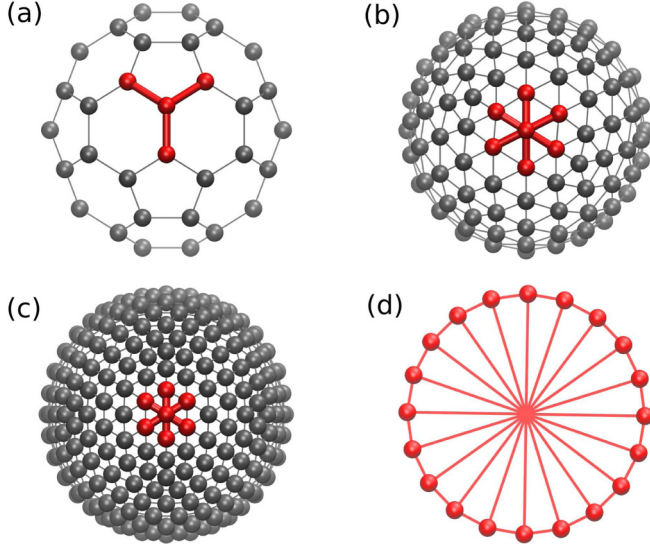


FIG. 1. (Color online) Spherical colloids composed of discrete mass points with the surface densities (a)  $\sigma a^2 = 0.53$ , (b)  $\sigma a^2 = 1.43$ , and (c)  $\sigma a^2 = 3.2$ . For illustration, the bonds of a particle and its nearest neighbors are highlighted in red. (d) Bonds in an equatorial plane connecting diametrically opposed particles for  $\sigma a^2 = 1.43$ .

The paper is organized as follows. The colloidal model and the MPC approach are described in Sec. II. Results for the translational and rotational velocity correlation functions are presented in Sec. III and the respective diffusion coefficients are determined. In Sec. IV the results of the discrete-shell sphere are compared with correlations for a solid sphere. Flow velocities and the flow field of a sedimenting colloid are shown in Sec. V. Finally, Sec. VI summarizes our findings.

## II. MODEL

### A. Spherical colloid

The colloid is modeled as a set of  $N_s$  point particles of mass  $M$  distributed over a spherical shell of radius  $R$ , which are tightly linked with each other to maintain a nearly rigid shape (cf. Fig. 1). The actual number of points depends on the radius of the colloid. Here a suitable number of points has to be chosen in order to achieve proper hydrodynamic behavior. We start out with a truncated icosahedron with a particle at every vertex. Higher surface densities are constructed by dividing the faces of the icosahedron of side length  $d$  into equilateral triangles of side length  $d/n$ , where  $n$  is an integer (here we use  $n = 4$  and 6). The mass points added at the polyhedrons are displaced radially from the center until they lie on a shell of radius  $R$ .

The mass points are connected with their nearest neighbors and with the diametrically opposite point particle via the harmonic potential

$$U(r) = \frac{K}{2}(r - r_0)^2, \quad (1)$$

where  $r = |\mathbf{r}|$  is the distance between two particles and  $\mathbf{r}$  the respective difference vector. Here  $r_0$  depends on the particular pair and is determined by the above described construction principle. The dynamics of a colloid particle is described by

Newton's equations of motion, which are solved by the velocity Verlet algorithm [45,46]. In addition, we perform simulations of a hard-sphere colloid of radius  $R$  with no-slip boundary conditions.

### B. Multiparticle collision dynamics fluid

The MPC fluid is composed of  $N$  point particles of mass  $m$  with the positions  $\mathbf{r}_i$  and velocities  $\mathbf{v}_i$  ( $i = 1, \dots, N$ ). The algorithm comprises two steps: a streaming and a collision step. In the streaming step, the particles move ballistically during a time increment  $h$ , which is called collision time, hence

$$\mathbf{r}_i(t+h) = \mathbf{r}_i(t) + h\mathbf{v}_i(t). \quad (2)$$

In the collision step, the simulation box is divided into cubic cells of side length  $a$  and the particle velocities in a collision cell are changed by a momentum-conserving stochastic process. Various collision rules have been proposed by now [10,32,47]. Here we use two different variants: a non-angular-momentum-conserving method, often referred to as stochastic rotation dynamics (SRD), and an angular-momentum-conserving approach as described in Ref. [32] based on Gaussian-distributed random velocities [47]. This allows us to analyze the influence of angular momentum conservation on (some) colloid correlation functions. We would like to point out that there are also angular-momentum-conserving variants of the SRD approach [48,49].

#### 1. Non-angular-momentum-conserving MPC

In this approach the velocity of the particle  $i$  is updated according to

$$\mathbf{v}_i(t+h) = \mathbf{v}_i(t) + [\mathbf{R}(\alpha) - \mathbf{E}][\mathbf{v}_i(t) - \mathbf{v}_{\text{c.m.}}(t)], \quad (3)$$

where

$$\mathbf{v}_{\text{c.m.}}(t) = \frac{1}{N_c} \sum_{j=1}^{N_c} \mathbf{v}_j(t) \quad (4)$$

is the velocity of the center of mass of the  $N_c$  particles in the cell that contains particle  $i$ ,  $\mathbf{R}(\alpha)$  is a rotation matrix for the rotation by the angle  $\alpha$ , and  $\mathbf{E}$  is the unit matrix [47,50]. The rotation angle  $\alpha$  is fixed, while the rotation axis is randomly oriented for each cell and collision. In addition, a random shift of the collision lattice is applied at every collision step in order to guarantee Galilean invariance [17]. The viscosity can be accurately predicted in terms of  $\alpha$ ,  $N_c$ , and  $h$  [11,12,17,19,20,22,48].

#### 2. Angular-momentum-conserving MPC

In the simulation of the hard-sphere colloid, an angular-momentum-conserving variant of MPC is used. Here the collision rule is [32,47]

$$\begin{aligned} \mathbf{v}_i(t+h) = & \mathbf{v}_{\text{c.m.}}(t) + \mathbf{v}_i^r - \frac{1}{N_c} \sum_{j=1}^{N_c} \mathbf{v}_j^r \\ & + m\mathbf{\Pi}^{-1} \sum_{j=1}^{N_c} [\mathbf{r}_{j,c} \times (\mathbf{v}_j - \mathbf{v}_j^r)] \times \mathbf{r}_{i,c}, \end{aligned} \quad (5)$$

where  $\mathbf{\Pi}$  is the moment-of-inertia tensor and  $\mathbf{r}_{i,c}$  is the relative particle position with respect to the center-of-mass position  $\mathbf{r}_{c.m.}$  of all the particles in the cell, i.e.,  $\mathbf{r}_{i,c} = \mathbf{r}_i - \mathbf{r}_{c.m.}$ . The velocities  $\mathbf{v}_i^r$  are chosen from a Maxwell-Boltzmann distribution of zero mean and variance  $k_B T/m$ .

### C. Colloid fluid coupling

#### 1. Non-angular-momentum-conserving MPC

The coupling between the MPC fluid and the colloid is established in the collision step, where the point particles of the sphere are treated similarly to fluid particles, however with a different mass  $M$  [14,16,24]. Hence, the velocities of the colloid point particles after collision are determined according to Eq. (3), but with the center-of-mass velocity

$$\mathbf{v}_{c.m.}(t) = \frac{\sum_{i=1}^{N_c} m \mathbf{v}_i(t) + \sum_{k=1}^{N_c^p} M \hat{\mathbf{V}}_k(t)}{m N_c + M N_c^p}. \quad (6)$$

Here  $N_c^p$  is the number of colloid point particles in the particular collision cell. The velocities  $\hat{\mathbf{V}}_k(t)$  are the velocities after streaming, which are not necessarily equal to those following from the previous collision step due to particle propagation by molecular dynamics simulations in the collision-time interval. Similarly, in cells with colloid point particles, Eq. (6) is applied for the calculation of the velocity of a fluid particle.

The fluid particles freely penetrate the sphere surface. The collisional coupling already suffices to drag internal fluid particles along with the moving colloid. We even satisfactorily achieve no-slip boundary conditions, as will be demonstrated in Sec. V.

A local Maxwellian thermostat, referred to as the Maxwell-Boltzmann scaling method, is used to maintain the temperature of the system at the desired value [50]. Thereby, the relative velocities  $\Delta \mathbf{v}_i$  and  $\Delta \mathbf{V}_k$  of all particles in a particular collision cell, with respect to the center-of-mass velocity of that cell, after a collision are scaled by a suitable factor. The scaling factor itself is given by  $[2E/(\sum_{i=1}^{N_c} m \Delta \mathbf{v}_i^2 + \sum_{k=1}^{N_c^p} M \Delta \mathbf{V}_k^2)]^{1/2}$ , where  $E$  is taken from the distribution function of the kinetic energy, which is divided by the actual cell relative kinetic energy.

#### 2. Angular-momentum-conserving MPC

The hard-sphere colloid moves ballistically during the collision-time interval  $h$ . The coupling between the MPC fluid and the hard-sphere colloid is achieved in two ways. After the colloid translation and rotation, the bounceback rule is applied for the streaming fluid particles [34,51]. Hence, here fluid particles are prevented from penetrating into the sphere volume. Moreover, phantom particles are taken into account in the collision step to minimize slip, which are located within a layer of thickness  $\sqrt{3}a$  underneath the sphere surface [32,52].

### D. Parameters

Three-dimensional periodic boundary conditions are applied for the MPC fluid, with a cubic simulation box of side length  $L = 90a$ , if not otherwise stated. We choose the average number of fluid particles per collision cell  $\langle N_c \rangle = 10$  and the collision angle as  $\alpha = 130^\circ$ . The collision times  $h = 0.1t_0$  and

$0.02t_0$  are considered, where  $t_0 = \sqrt{ma^2/k_B T}$  is the time unit of the MPC fluid, which yields the viscosities  $\eta/\sqrt{mk_B T/a^4} = 8.7$  and  $41.2$ , where  $k_B$  is Boltzmann's constant and  $T$  the temperature. In the simulation we set  $a = 1$ ,  $m = 1$ , and  $k_B T = 1$ .

The time step  $\Delta t = 0.002t_0$  is applied for the integration of Newton's equations of motion of the point particles of mass  $M = 10m$  comprising a colloid. The latter mass has been shown to lead to an adequate fluid-particle coupling, necessary for the appearance of hydrodynamic behavior [53]. We select a large spring constant  $K = 5000k_B T/a^2$  to closely maintain a spherical shape. The radius of the sphere is set to  $R = 3a$  and the three surface densities  $\sigma a^2 = 0.53, 1.43$ , and  $3.2$  are considered. The latter corresponds to  $N_s = 60, 162$ , and  $362$  surface particles (cf. Fig. 1). We expect that the radius  $R = 3a$  is large enough to yield results that are only marginally affected by the underlying discrete fluid simulation approach [31].

Eight independent simulation runs of typically  $5600t_D$  were performed for every system, where  $t_D = 6\pi\eta R^3/k_B T$  is the diffusion time of a hard-sphere colloid. This corresponds to  $2.5 \times 10^7$  MPC collisions for systems with  $h = 0.1t_0$ .

The systems are efficiently simulated by a combination of a GPU and a CPU [54]. Thereby, the fluid dynamics is managed by a GPU-based code and the colloid dynamics is integrated by a CPU.

For the simulation of the hard-sphere colloid via the angular-momentum-conserving MPC fluid, the collision time step is  $h = 0.0425t_0$ . We assume a buoyant colloid, hence its total mass is  $M_c = 4\pi m \langle N_c \rangle R^3/3a^3$ . To determine the viscosity of the fluid, we performed nonequilibrium simulations with a sinusoidal force profile applied in the  $x$  direction of the Cartesian reference frame. Explicitly, the force on a fluid particle is

$$f_{ix} = F \cos(qr_{iy}), \quad (7)$$

with the wave vector  $q = 2\pi/L$ . As discussed in Ref. [45], the appearing velocity profile  $u_x$  is related to the fluid viscosity according to

$$u_x(r_y) = \frac{\langle N_c \rangle}{q^2 \eta a^3} f_x(r_y). \quad (8)$$

Using the value  $F/(k_B T/a) = 5 \times 10^{-4}$ , which yields sufficiently small velocities  $|u_x|/\sqrt{k_B T/m} < 0.01$  to be in the linear response regime, we obtain the viscosity  $\eta/\sqrt{mk_B T/a^4} = 7.8$ . Comparing this value with the theoretical prediction for this MPC algorithm [48], we find that the above value extracted from the simulation is approximately 10% smaller.

## III. DYNAMICS OF THE POINT-PARTICLE SPHERE

### A. Center-of-mass displacement

Center-of-mass mean square displacements of the discrete-particle colloids are presented in Fig. 2 for the various surface densities. In the asymptotic limit of long times, we find linearly increasing mean square displacements. The various colloidal masses are reflected at short times, where we find a strong ballistic dynamics for the largest density (mass) and a somewhat smaller initial slope for the smallest surface density.

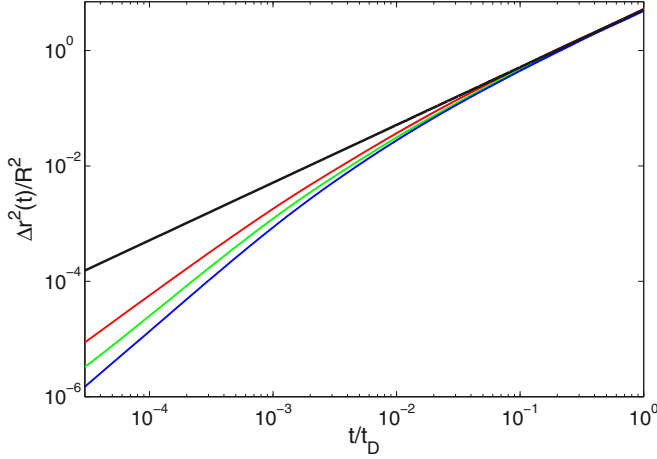


FIG. 2. (Color online) Mean square displacements of the center of mass of spheres with the surface particle densities  $\sigma a^2 = 0.53$ , 1.43, and 3.2 (top to bottom), i.e.,  $N_s = 60$ , 162, and 362, and the collision time step  $h = 0.1t_0$ . The straight line represents the asymptotic linear dependence  $6D_T t$ , with  $D_T$  values given in Table I;  $t_D = 6\pi\eta R^3/k_B T$ .

The translational diffusion coefficients extracted from the asymptotic linear time dependence of the finite-size system are presented in Table I. They are normalized by the diffusion coefficient  $D_T^0 = k_B T / 6\pi\eta R$  of a hard sphere with no-slip boundary conditions. The diffusion coefficients exhibit a moderate dependence on the surface density, with larger  $D_T$  for lower densities. There is also a small difference between the diffusion-coefficient ratios for the two collision time steps. Overall, however, the values agree well.

As is well known, the translational diffusion coefficient is strongly influenced by finite-size effects. This is reflected by the fact that the diffusion-coefficient ratios of Table I are considerably smaller than unity. We will address this issue in Sec. III D in more detail.

### B. Translational velocity autocorrelation function

The center-of-mass velocity autocorrelation function (VACF) of a colloid

$$C_T(t) = \langle \mathbf{V}(t) \cdot \mathbf{V}(0) \rangle, \quad (9)$$

with

$$\mathbf{V} = \frac{1}{N_s} \sum_{i=1}^{N_s} \mathbf{V}_i \quad (10)$$

TABLE I. Center-of-mass diffusion coefficients extracted from the mean square displacements of Fig. 2 for the collision times  $h_1 = 0.1t_0$  and  $h_2 = 0.02t_0$ ;  $D_T^0 = k_B T / 6\pi\eta R$ .

$\sigma a^2$	$D_{T,h_1}/D_T^0$	$D_{T,h_2}/D_T^0$
0.53	0.86	0.94
1.43	0.84	0.87
3.2	0.81	0.8

its center-of-mass velocity and  $\mathbf{V}_i$  the velocity of the colloid surface particle  $i$ , shows several regimes [13,36,55]. As indicated in Fig. 2, inertia effects play a role at short times and hydrodynamic correlations over the length scale of the colloid have buildup only for times larger than the viscous time scale

$$\tau_v = \frac{(2R)^2}{\nu}. \quad (11)$$

Here  $\nu = \eta/\rho$  is the kinematic viscosity and  $\rho = m\langle N_c \rangle/a^3$  the fluid mass density. For the collision time steps  $h = 0.1t_0$  and  $0.02t_0$ , the viscous times are  $\tau_v/t_0 \approx 41$  and 9 or  $\tau_v/t_D \approx 10^{-2}$  and  $4 \times 10^{-4}$ , respectively. Moreover, sound propagation affects the correlation function because the MPC fluid is compressible [13]. This complicates the disentanglement of the various contributions to the correlation function.

#### 1. Short-time collisional regime

Within the molecular-chaos assumption, i.e., in the absence of hydrodynamic correlations, a center-of-mass VACF of a sphere can be determined analytically as shown in Appendix A. The result is

$$C_T(t) = \frac{3k_B T}{MN_s} (1 - \mu)^{t/h}, \quad (12)$$

with

$$\mu = \frac{2}{3} (1 - \cos \alpha) \frac{m\langle N_c \rangle}{m\langle N_c \rangle + kM}, \quad (13)$$

as previously discussed for polymers [23] (for a MPC fluid see Refs. [53,56]). Here  $k$  denotes the (average) number of colloid surface mass points in a collision cell. Equation (12) can be written as

$$C_T(t) = C_T(0) e^{-t/\tau_c}, \quad (14)$$

with the relaxation time

$$\tau_c = -\frac{h}{\ln(1 - \mu)}. \quad (15)$$

Since the initial velocities are independent, i.e., the molecular-chaos assumption applies, we expect that the decay of the correlation function after one step is described by Eq. (14). The extent to which agreement is obtained for longer times depends on the collision time step [53]. For the considered small time steps, we expect agreement for the first step only.

Figure 3 confirms the expected behavior for the first collision. *A priori*, it is not evident how many surface points are in a collision cell. For the lowest density, there is approximately one point in a cell, i.e.,  $k = 1$ . The slower decay for the other densities is related to a higher surface particle concentration in a cell. By inverting Eq. (15), we extract an effective mass  $M_e = kM$  in terms of the measured time  $\tau_c(h)$ . The corresponding values  $M_e$  are listed in Table II. It is interesting to note that  $M_e$  is roughly proportional to  $\sigma$  when  $\sigma a^2 > 1$ , as expected.

To confirm our theoretical considerations, we performed Brownian MPC simulations, i.e., MPC simulations without momentum conservation [23]. Here the buildup of hydrodynamic correlations is suppressed by assigning a fluid phantom particle to every colloid point particle, where the phantom

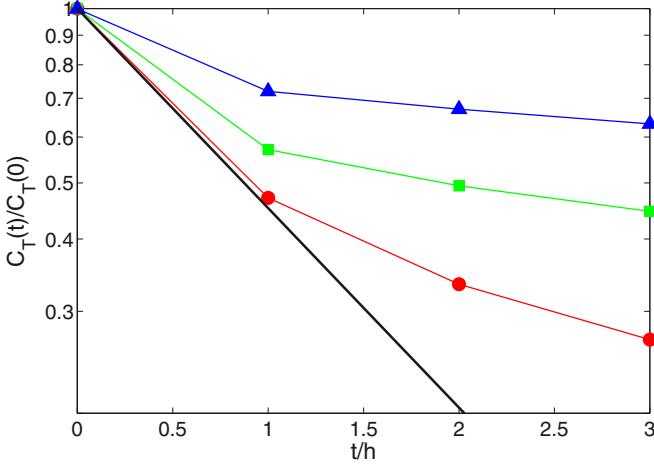


FIG. 3. (Color online) Short-time center-of-mass velocity auto-correlation functions for the surface particle densities  $\sigma a^2 = 0.53$  (bullets), 1.43 (squares), and 3.2 (triangles) (cf. Fig. 1). The line corresponds to the exponential decay (14) with  $\tau_c$  calculated according to Eq. (15) for  $k = 1$ .

particles velocity is taken from a Gaussian distributed with zero mean and variance  $k_B T/M$ . As expected, the obtained correlation functions decay exponentially according to the theoretical prediction (14).

Already for the second collision step ( $t = 2h$ ), we observe considerable deviations from an exponential decay in Fig. 3, which is related to the buildup of hydrodynamic correlations, i.e., correlations build up rather fast. The initial exponential decay of the VACF of a solid colloid is typically described by Enskog kinetic theory [31,34,36,55,57–61], with the relaxation time [34]

$$\tau_E^{-1} = \frac{16}{3M_c a^3} \sqrt{2\pi k_B T m \langle N_c \rangle} R^2 \quad (16)$$

for a colloidal with no-slip boundary conditions and mass  $M_c \gg m$ . The relaxation time  $\tau_E \approx 1t_0$  is much longer than the relaxation time  $\tau_c = 0.126t_0$  for  $\sigma = 0.53a^2$  [Eq. (15)]. Thus, the initial decay is not described by Enskog friction. A suitable expression describing the correlation function over the initial time interval (several collisions) remains to be theoretically derived.

## 2. Hydrodynamic regime

*a. Theoretical consideration: Hard-sphere colloid.* Hydrodynamic interactions imply particular correlations in the dynamics of a colloidal particle, which can be captured by the

TABLE II. Collisional decay times  $\tau_c$  and effective masses  $M_e = kM$  for  $h_1 = 0.1t_0$  and  $h_2 = 0.02t_0$ . The decay time of an individual particle of mass  $M = 10m$  is  $\tau_{c,h_1} = 0.13t_0$ .

$\sigma a^2$	$\tau_{c,h_1}/t_0$	$M_{e,h_1}/m$	$\tau_{c,h_2}/t_0$	$M_{e,h_2}/m$
0.53	0.13	10.7	0.027	10.7
1.43	0.18	15.5	0.035	15
3.2	0.3	29.2	0.058	27

generalized Langevin equation

$$M_c \dot{V}(t) = - \int_0^t \gamma(t-s) V(s) ds + \Gamma(t), \quad (17)$$

with the memory function  $\gamma(t)$  and the white-noise random force  $\Gamma(t)$  [62–65]. The VACF is then given by

$$C_T(t) = \frac{3k_B T}{2\pi} \int_{-\infty}^{\infty} \frac{e^{-i\omega t}}{\gamma(\omega) - i\omega M_c} d\omega, \quad (18)$$

with the frequency-dependent friction coefficient  $\gamma(\omega)$  [36,66,67]. A purely hydrodynamic expression for  $\gamma(\omega)$  can be obtained from the Navier-Stokes equations with proper boundary conditions on the sphere surface, i.e., the fluid is considered as a continuum and hydrodynamics applies down to infinitely small length and time scales [62,68]. (The latter does not apply for the MPC fluid [13].) This yields for no-slip boundary conditions [66,67,69]

$$\gamma(\omega) = \frac{4\pi}{3} \eta R x^2 \frac{(1+x)(9-9i\zeta-2\zeta^2) + x^2(1-i\zeta)}{2x^2(1-i\zeta) - (1+x)\zeta^2 - x^2\zeta^2}, \quad (19)$$

with the abbreviations  $x = R\sqrt{-i\omega\rho/\eta}$ ,  $\zeta = \omega R/\hat{c}$ ,  $\hat{c} = \sqrt{c^2 - i4\omega\eta/3\rho}$ , and  $c$  the velocity of sound.

*b. Theoretical consideration: Point-particle colloid.* Alternatively, an approximate theoretical expression for the translational VACF can be obtained by a fluctuating hydrodynamics approach in analogy to the treatment of a polymer [70]. For the coupling of the sphere to the fluid, we assume no-slip boundary conditions, i.e., the velocities of the surface particles are equal to the local fluid velocity. The fluid velocity field itself is given by the solution of the linearized Landau-Lifshitz Navier-Stokes equations [13,70,71]. Neglecting the hydrodynamic coupling between internal degrees of freedom, the center-of-mass velocity of our sphere of point particles is then given by

$$V(t) = \frac{1}{N_s} \sum_{i=1}^{N_s} v^R(\mathbf{R}_i, t), \quad (20)$$

where  $v^R(\mathbf{R}_i, t)$  is the random fluid velocity induced by the thermal fluctuations in the fluid (a white-noise force density) at the position  $\mathbf{R}_i$  of a sphere-surface particle and time  $t$ . The correlation function of the random velocity within the linearized Landau-Lifshitz Navier-Stokes equations has been calculated in Ref. [13], which yields [13,70]

$$C_T(t) = \frac{1}{N_s} \frac{k_B T}{V} \sum_{\mathbf{k}} S(\mathbf{k}) [2Q^T(\mathbf{k}, t) + Q^L(\mathbf{k}, t)] \quad (21)$$

for a finite periodic simulation box of volume  $V$ , with the wave-vector components  $k_\beta = 2\pi n_\beta/L$ ,  $n_\beta \in \mathbb{Z}$ ,  $\mathbf{k} \neq 0$ , and  $\beta \in \{x, y, z\}$ . Here  $S$  denotes the structure factor

$$S(\mathbf{k}) = \frac{1}{N_s} \sum_{i=1}^{N_s} \sum_{j=1}^{N_s} \langle e^{i\mathbf{k} \cdot (\mathbf{R}_i - \mathbf{R}_j)} \rangle, \quad (22)$$

where the sum is performed over the discrete sphere-surface particles. In the exponent of Eq. (22), we neglect the time dependence because the dynamics of the colloid is by far slower than that of the fluid particles. The terms  $Q^T$  and  $Q^L$  are

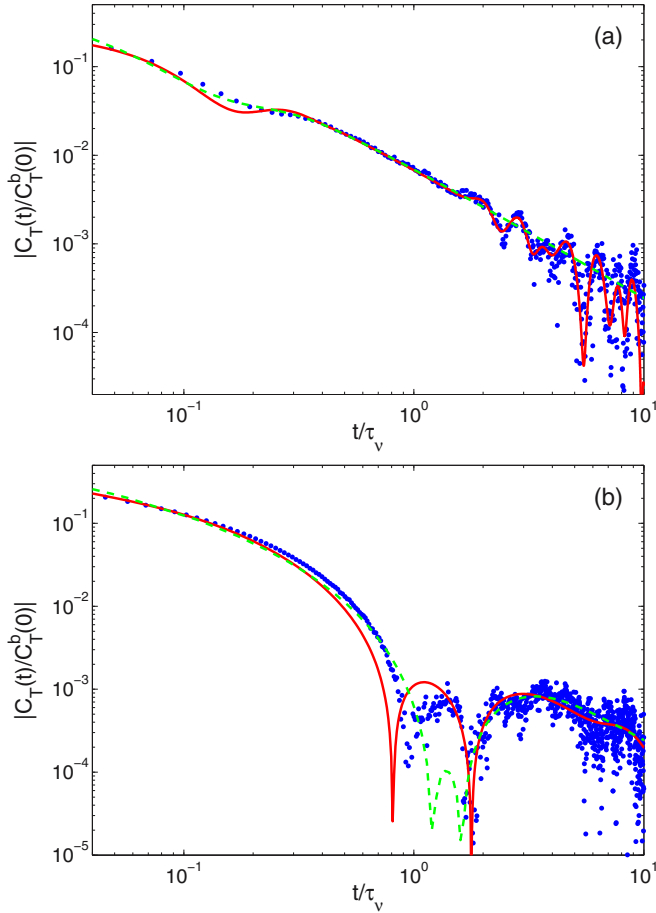


FIG. 4. (Color online) Colloid center-of-mass VACF (blue dots) compared with the analytical results for a neutrally buoyant hard-sphere colloid according to Eq. (18) (green dashed line) and the analytical result (21) (red solid line) for the surface density  $\sigma a^2 = 0.53$  and (a)  $h = 0.1t_0$  and (b)  $h = 0.02t_0$ . Here  $C_T(t)$  is normalized by the value  $C_T^b(0) = 3k_B T/M_c$  of a neutrally buoyant hard-sphere colloid.

the hydrodynamic tensors for the transversal and longitudinal hydrodynamic modes [13]; they are explicitly provided in Appendix B. As for the above solid-colloid description, this approach applies above a minimum length scale only, since again the continuum solution of the Navier-Stokes equations is used, which does not apply to the MPC fluid below a minimum length scale [13].

*c. Simulation results.* Figure 4 shows VACFs for the surface density  $\sigma = 0.53/a^2$  and two collision time steps. The correlation functions decay nonexponentially and exhibit a long-time tail. At  $t = 0$ , the simulations yield the equipartition value  $C_T(0) = 3k_B T/N_s M$ . Since the MPC fluid is compressible, we find a first signature of sound propagation at  $t/\tau_v \approx 0.2$  and  $t/\tau_v \approx 1$  for  $h = 0.1t_0$  and  $0.02t_0$ , respectively, corresponding to the time required for sound to cover the diameter of a colloid. Thereby, the backtracking effect is more pronounced for  $h = 0.02t_0$ , where the correlation function assumes negative values [13]. Further sound undulations are visible in Fig. 4(a) for  $t/\tau_v \gtrsim 2$ , in accord with the time required for sound to traverse the simulation box, i.e.,  $t_s \approx L/c$ .

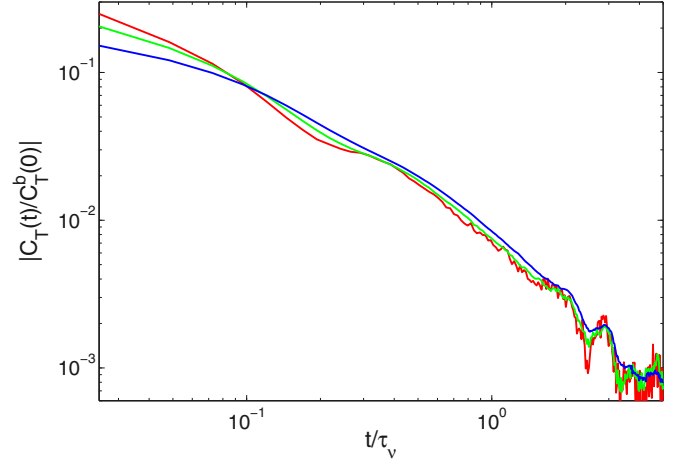


FIG. 5. (Color online) Colloid center-of-mass VACFs for the surface densities  $\sigma a^2 = 0.53$  (red line),  $1.43$  (green line), and  $3.2$  (blue line) and  $h = 0.1t_0$ .

The simulation results of Fig. 4(a) are well described by the theoretical expressions (18) and (21) above  $t/\tau_v \approx 0.4$ . The expression (21) even reproduces the long-time sound undulations. Both theoretical curves turn into the long-time tail  $C_T(t) = k_B T/4\rho(\pi vt)^{3/2}$  [13] for  $t/\tau_v > 10$ , which is solely determined by fluid properties. However, the backtracking effect is not reproduced well. For very short times, an improved MPC-related analytical expression has to be derived.

Figure 5 compares correlation functions for various surface densities. There is a slight but systematic increase of  $C_T(t)$  with  $\sigma$  for  $t/\tau_v \gtrsim 0.4$  due to inertia effects of the colloids of different mass. For the lowest surface density, inertia seems to be of minor importance.

In order to elucidate the influence of the mass  $M$  of a point particle and their concentration on the correlation function, we present in Fig. 6 results for the surface densities  $\sigma = 0.53/a^2$  with  $M = 60.3m$  and  $\sigma = 3.2/a^2$  with  $M = 10m$ , which correspond to a total colloid mass of  $3620m$ . Similarly, we compare simulations for systems with  $\sigma = 3.2/a^2$  and  $M = 1.66m$  to those with  $\sigma = 0.53/a^2$  and  $M = 10m$ , which correspond to a total mass of  $600m$ . The VACFs for the systems with the same total colloid mass agree with each other above a certain time. The difference between the curves for the low- and high-mass systems is expected, as indicated in Fig. 5, and is in qualitative agreement with the theoretical expression (18). For shorter times, however, the VACF of the high-mass simulations deviates slightly, which could be a sound effect, or due to a different coupling with the MPC solvent.

### C. Angular velocity autocorrelation function

#### 1. Theoretical consideration: Hard-sphere colloid

The angular velocity autocorrelation function (AVACF) is defined as

$$C_R(t) = \langle \mathbf{\Omega}(t) \cdot \mathbf{\Omega}(0) \rangle \quad (23)$$

in terms of the angular velocity  $\mathbf{\Omega}$ , which is obtained from the relation

$$\mathbf{\Omega}(t) = \mathbf{I}^{-1} \mathbf{L}. \quad (24)$$

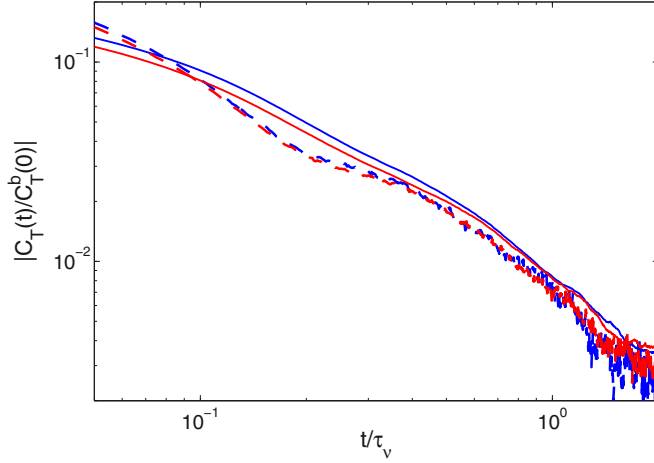


FIG. 6. (Color online) Colloid center-of mass VACFs for the surface densities  $\sigma a^2 = 0.53$  (blue line) and  $3.2$  (red line) and the point-particle masses  $M/m = 60.3$  and  $10$  (solid line), respectively, as well as  $M/m = 10$  and  $1.66$  (dashed line), respectively. This corresponds to the total mass of the colloids  $3620m$  (solid line) and  $600m$  (dashed line).

The moment of inertia tensor  $\mathbf{I}$ , with its magnitude  $I = |\mathbf{I}|$ , and the angular momentum  $\mathbf{L}$  are calculated in a reference frame located at the center of mass of the sphere.

As the translational velocity autocorrelation function,  $C_R$  exhibits an initial collisional regime, which decays in the same way as  $C_T(t)$  [cf. Eqs. (14) and (15) and Fig. 3]. An analytical expression for the AVACF of a colloid immersed in a fluid has been derived in Refs. [72,73]. In terms of the Laplace transformation, it is given by

$$C_R(t) = \frac{1}{2\pi i} \int e^{st} \left( s + \frac{\gamma_R(s)}{I} \right)^{-1} ds \quad (25)$$

for a colloid with stick boundary conditions, with the rotational friction coefficient

$$\gamma_R(s) = 8\pi\eta R^3 \left( 1 + \frac{\rho R^2 s / \eta}{3(1 + \sqrt{\rho R^2 s / \eta})} \right). \quad (26)$$

## 2. Simulation results

Figure 7 shows simulation results for the two applied collision time steps, i.e., AVACFs for two viscosities. Evidently, the curves for the two collision-step sizes agree very well up to  $t/\tau_v \approx 2$ . For longer times, statistical fluctuations imply deviations. This stresses the fact that only transverse hydrodynamic modes play a role in the rotational behavior of a sphere.

The analytical expression (25) is compared with simulation results for various surface densities in Fig. 8. The agreement is good for the lower surface densities. For the highest density, we find a somewhat stronger decay of the AVACF at longer times. In any case, the correlation functions seem to follow the long-time tail power-law decay  $t^{-5/2}$ . At short times, we find deviations from the theoretical result, which are related to the initial nonhydrodynamic decay of the correlation function.

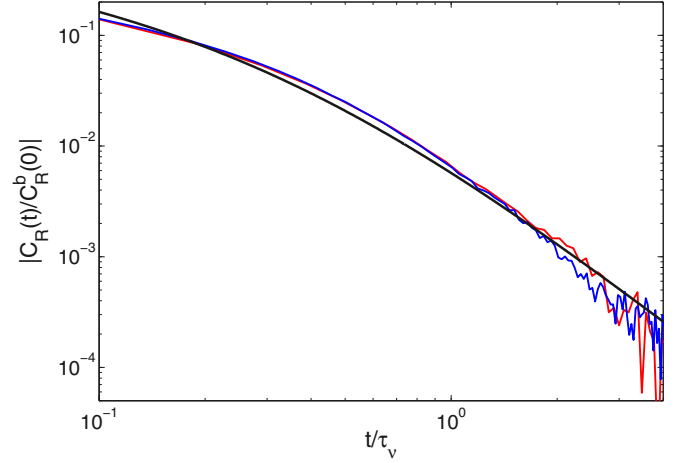


FIG. 7. (Color online) Angular velocity autocorrelation functions of a spherical colloid for the viscosities  $\eta/\sqrt{mk_B T/a^4} = 8.7$  ( $h = 0.1t_0$ , red line) and  $41.2$  ( $h = 0.02t_0$ , blue line). The particle surface density is  $\sigma/a^2 = 0.53$ . The black line corresponds to the analytical expression (25).

## D. Diffusion coefficient

The Green-Kubo relation

$$D_\Lambda = \frac{1}{3} \int_0^\infty C_\Lambda(t) dt \quad (27)$$

yields the diffusion coefficient from the correlation function for translation  $\Lambda = T$  and rotation  $\Lambda = R$ . In general, the translational diffusion coefficient comprises local frictional and hydrodynamic  $D_T^H$  contributions, i.e.,

$$D_T = \frac{D_0}{N_s} + D_T^H. \quad (28)$$

Without hydrodynamic correlations, the total friction coefficient of a sphere is the sum of the contributions of the individual point particles. Hence,  $D_0/N_s$  is the overall

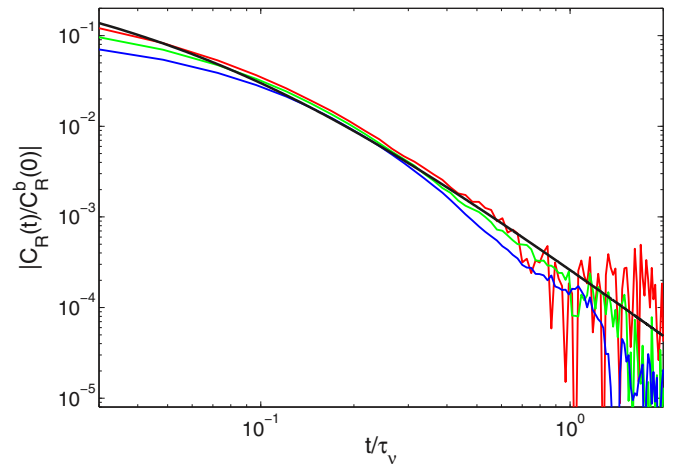


FIG. 8. (Color online) Angular velocity autocorrelation functions of a spherical colloid for the surface densities  $\sigma a^2 = 0.53$  (red line),  $1.43$  (green line), and  $3.2$  (blue line) and the MPC collision time  $h = 0.1t_0$ . The black line indicates the analytical expression (25).

TABLE III. Rotational diffusion coefficients and hydrodynamic radii for a sphere of radius  $R = 3a$  for various surface densities  $\sigma$  and the collision time steps  $h_1 = 0.1t_0$  and  $h_2 = 0.02t_0$ ;  $D_R^0 = k_B T / 8\pi\eta R^3$ .

$\sigma a^2$	$D_{R,h_1}/D_R^0$	$R_{H,h_1}/a$	$D_{R,h_2}/D_R^0$	$R_{H,h_2}/a$
0.53	0.94	3.1	1.06	3.0
1.43	0.71	3.4	0.75	3.3
3.2	0.5	3.8	0.53	3.7

diffusion coefficient by local friction, with the diffusion coefficient  $D_0$  of an individual surface mass point.

The hydrodynamic radius of a colloid follows from the translational and rotational diffusion coefficients via the relations

$$D_T^H = \frac{k_B T}{6\pi\eta R_H}, \quad (29)$$

$$D_R = \frac{k_B T}{8\pi\eta R_H^3}. \quad (30)$$

Table III presents rotational diffusion coefficients and the corresponding hydrodynamic radii for various surface densities. They are normalized by the rotational diffusion coefficient  $D_R^0 = k_B T / 8\pi\eta R^3$  of a hard sphere.

The translational diffusion coefficient depends on system size  $L$ , whereas the decay of the rotational correlation function is fast enough such that  $D_R$  is essentially independent of  $L$ . In order to determine diffusion coefficients in the asymptotic limit of an infinite box size, we performed simulations for the system sizes  $L = 30a$ ,  $50a$ , and  $90a$ . The autocorrelation functions are shown in Fig. 9. With increasing system size, the sound modes at  $t_s = L/c$  of the VACF shift to longer times, whereas the short-time behavior ( $t/\tau_v < 0.1$ ) is unaffected by the system size. The analytical expression (21) qualitatively captures the time dependence for small box sizes and quantitatively describes the VACF above  $t/\tau_v \approx 0.4$  for the largest considered box size  $L = 90a$ .

No sound effects are present in the AVACF and the correlation function is nearly independent of system size. The analytical expression (25) describes the simulation data well above  $t/\tau_v = 0.1$ . The diffusion coefficients determined by the integrals (27) are displayed in Table IV. The diffusion coefficient  $D_T$  clearly increases with increasing system size, whereas  $D_R$  is constant.

Assuming pointlike particles, the long-range hydrodynamic correction for the diffusion coefficient in a periodic system can be calculated analytically, which yields [74,75]

$$D_T^H(L) = D_T^H(\infty) - 2.837 \frac{k_B T}{6\pi\eta L}, \quad (31)$$

where  $D_T^H(\infty)$  is the hydrodynamic part of the translational diffusion coefficient of the infinite system. Table IV lists the diffusion coefficients  $D_T$  obtained from integration of the correlation functions (27). With the numerically determined diffusion coefficient  $D_0/\sqrt{k_B T a^2/m} = 0.02$  of a MPC particle of mass  $M = 10m$ , we obtain the respective coefficients  $D_T^H$ . A fit of the expression (31) to the finite-size  $D_T^H(L)$  values of Table IV yields the value  $D_T^H(\infty) = 0.88D_T^0$  and the

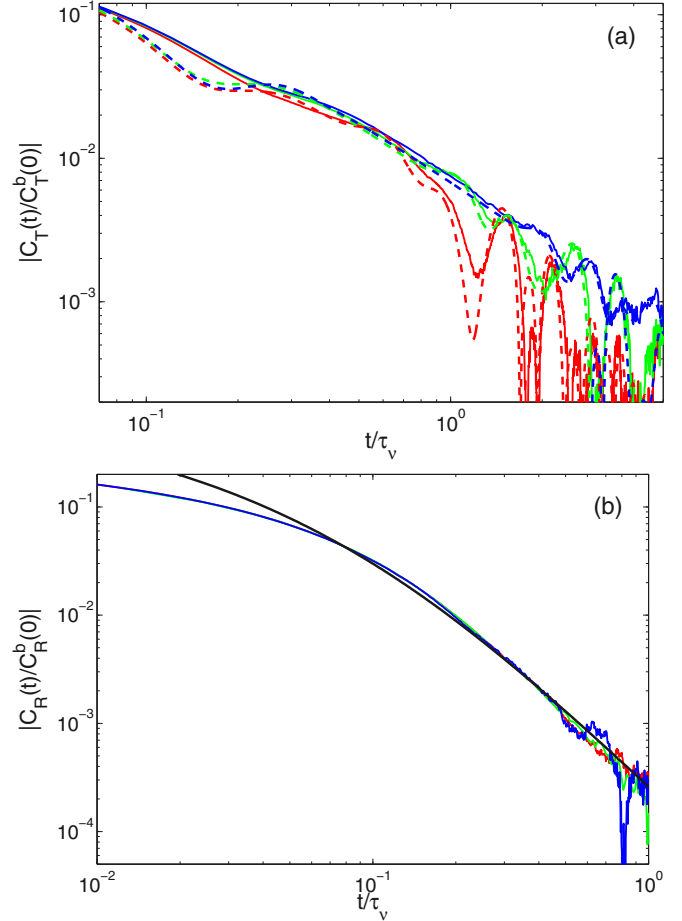


FIG. 9. (Color online) (a) Center-of-mass velocity autocorrelation functions and (b) angular velocity autocorrelation functions for the box sizes  $L/a = 30$  (red line),  $50$  (green line), and  $90$  (blue line). The surface density is  $\sigma a^2 = 1.43$  and  $h = 0.1t_0$ . The dashed lines in (a) are calculate via Eq. (21) and the smooth black line in (b) is calculated by Eq. (25).

hydrodynamic radius  $R_H = 3.4a$ . This value agrees very well with  $R_H^r$  extracted from the rotational diffusion coefficient.

Alternatively,  $D_T^H(\infty)$  can be obtained directly from the VACF [70]. As shown in Fig. 9, the colloid center-of-mass velocity autocorrelation function can be described quantitatively by the theoretical expression (21) above a certain time scale. To obtain the infinite-system-size correlation function, we suggest to replace the (oscillating) tail of the finite-size simulation result by the infinite-system analytical expression

TABLE IV. Translational  $D_T$  and rotational  $D_R$  diffusion coefficients and the respective hydrodynamic radii  $R_H$  and  $R_H^r$  for various simulation box sizes  $L$ ,  $\sigma = 1.43a^2$ , and  $h = 0.1t_0$ . The  $D_T^H$  are the hydrodynamic contributions to the translational diffusion coefficients [cf. Eq. (28)].

$L/a$	$D_T/D_T^0$	$D_T^H/D_T^0$	$R_H/a$	$D_R/D_R^0$	$R_H^r/a$
30	0.64	0.58	5.2	0.7	3.4
50	0.79	0.73	4.1	0.7	3.4
90	0.84	0.78	3.8	0.7	3.4
$\infty$	0.94	0.88	3.4	0.7	3.4

and integrate the combined correlation function to obtain the asymptotic value  $D_T^H(\infty)$ . This yields the diffusion coefficient  $D_T^H(\infty) = 0.91D_T^0$  and the hydrodynamic radius  $R_H = 3.3a$ . This value closely agrees with that presented in Table IV obtained by extrapolation.

The obtained hydrodynamic radii are all larger than the colloid size  $R$ . This is partly due to the hydrodynamic radius of the surface particles themselves. The diffusion coefficient  $D_0/\sqrt{k_B T a^2/m} = 0.02$  of a surface particle corresponds to the hydrodynamic radius  $r_H/a \approx 0.3$  [76], when we assume no-slip boundary conditions. Thus,  $R_H/a = 3.3$  or  $3.4$  is close to the sum of the sphere radius and the hydrodynamic radius of a surface particle.

#### IV. CORRELATION FUNCTIONS OF A SOLID COLLOID

Figure 10 shows the VACF and AVACF for a neutrally buoyant hard-sphere colloid and the colloid composed of discrete point particles in the MPC solvent. The viscosities of the two systems are different. However, we scale the time by

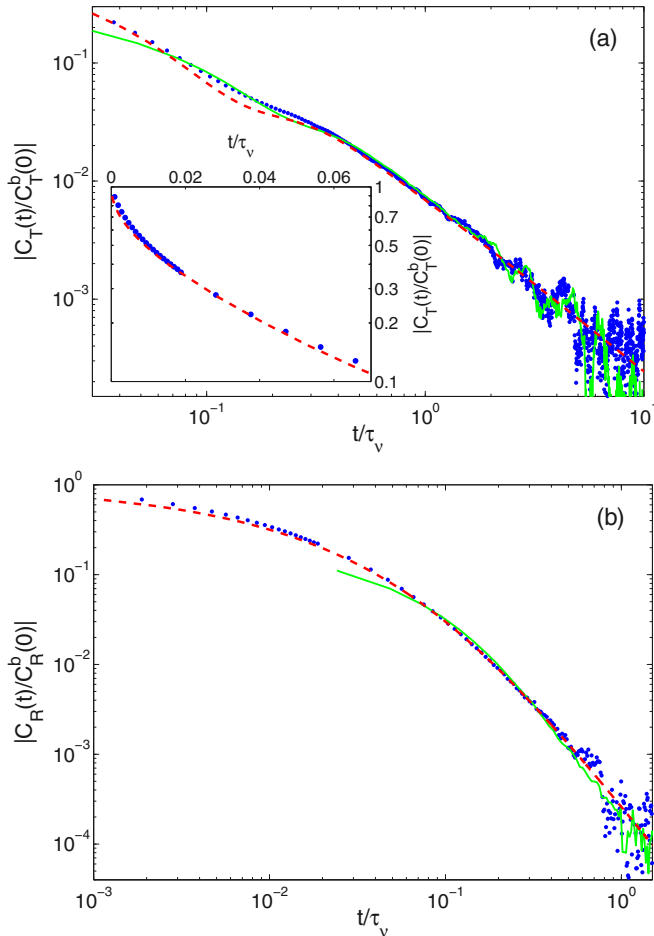


FIG. 10. (Color online) (a) Center-of-mass velocity autocorrelation functions and (b) rotational velocity autocorrelation functions for a neutrally buoyant hard sphere (blue dots) and a sphere composed of discrete point particles (green line) with the surface particle density  $\sigma = 1.43a^2$ . The dashed line (red) represents the theoretical expressions (18) and (25), respectively. The inset in (a) shows the nonexponential short-time behavior of the hard-sphere colloid correlation function.

$\tau_v$ , which removes the dependence on the viscosity, at least for long times. Evidently, the long-time behavior of both colloids is identical. However, we observe distinct model-specific differences for short times. Specifically, the sound contributions are somewhat different for the translational correlation function and there are even more pronounced differences for shorter times. The correlation functions obtained from simulation compare very well with the theoretical expressions (18) and (25) for an infinitely large system above  $t/\tau_v \approx 0.5$  and  $t/\tau_v \approx 10^{-2}$  for translation and rotation, respectively [see also Fig. 4(a)]. Finite-system-size effects appear for the  $C_T$  above  $t/\tau_v \approx 2$  [see Fig. 10(a)].

The inset of Fig. 10(a) shows the close agreement between the simulation data and the analytical expression (18) for short times. There is no evidence for an exponentially Enskog-type decaying correlation function. The VACF is distinct from an exponential function. The close agreement between the theory and simulation results suggests that due to our choice of boundary conditions at the colloid surface, i.e., taking into account phantom particles, hydrodynamics dominates the colloid dynamics even at very small time scales of a few MPC collisions [52]. We like to mention that both simulation and theory yield the equipartition value  $C_T(0) = 3k_B T/M_c$  in the static limit.

#### V. SEDIMENTATION

Finally, we study the fluid flow field around a sedimenting colloid composed of discrete point particles in the presence of an applied constant force  $f$ . A backflow of the fluid is introduced by a force on the fluid particles such that the total center-of-mass velocity of the system is zero [77]. Figure 11 shows the fluid velocity field in the vicinity of the sphere with  $\sigma = 1.43/a^2$  and  $h = 0.1t_0$  at the Reynolds number  $Re = uR/\nu \approx 0.25$ , where  $u$  is the average sedimentation velocity. The reference frame is fixed at the colloid center, hence fluid flows in the negative  $z$  direction, i.e., we subtract the average drift velocity of the colloid from the fluid velocity field. Due to the symmetry, we use cylindrical coordinates with the cylinder axis along the  $z$  axis of the Cartesian reference frame (sedimentation direction) and the radial coordinate  $r$ .

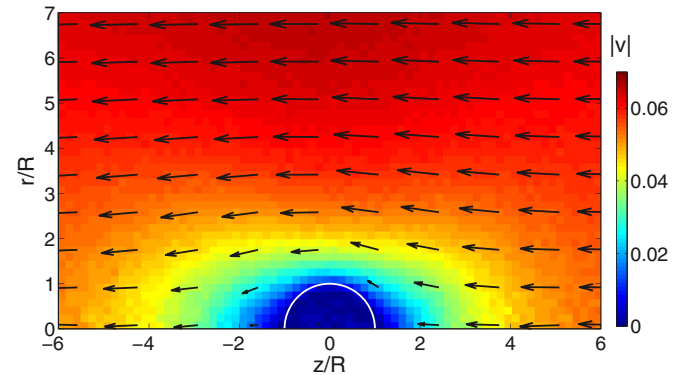


FIG. 11. (Color online) Fluid velocity field in the rest frame of a sedimenting colloid composed of discrete particles with the surface density  $\sigma a^2 = 1.43$  and  $h = 0.1t_0$ . Arrows indicate the direction of the velocity field  $\mathbf{v}$ . The magnitude of the field  $|\mathbf{v}|$  is color coded. Cylindrical coordinates are used, with the cylinder axis along the  $z$  axis of the Cartesian reference frame (sedimentation direction) and the radial coordinate  $r$ .

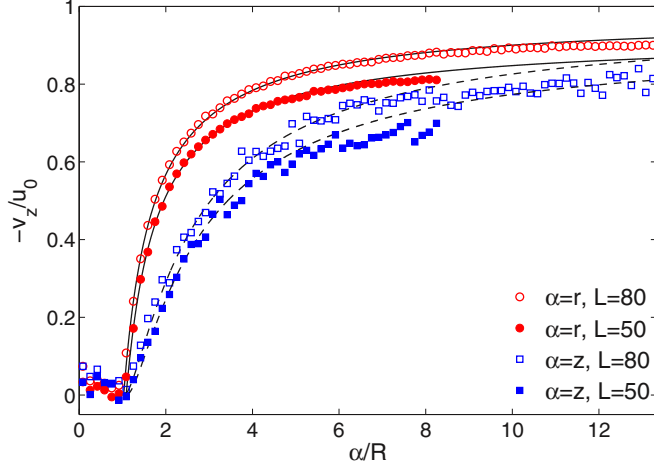


FIG. 12. (Color online) Comparison of the fluid velocity component  $v_z$  obtained from simulation (symbols) and calculated according to Eq. (32) (lines) along the sedimentation direction  $z$  (blue squares) and along the radial direction  $r$  (red circles). For the two system sizes  $L = 80$  (open symbols) and  $L = 50$  (closed symbols), we obtain the hydrodynamic radii  $R_H = 3.075a$  and  $3.25a$ , respectively. The system parameters are  $\sigma a^2 = 1.43$  and  $h = 0.1t_0$ . The velocities are scaled by the value  $u_0 = f/6\pi\eta R$ .

axis along the  $z$  axis of the Cartesian reference frame and the radial coordinate  $r$ .

The strength of the velocity field along the sedimentation and radial directions are displayed in Fig. 12 for two sizes of the periodic system. The numerical results are compared with the analytical expression

$$\mathbf{v} = \mathbf{u} - \frac{3}{4}R_H \frac{\mathbf{u} + \hat{\mathbf{r}}(\mathbf{u} \cdot \hat{\mathbf{r}})}{|\mathbf{r}|} - \frac{1}{4}R_H^3 \frac{\mathbf{u} - 3\hat{\mathbf{r}}(\mathbf{u} \cdot \hat{\mathbf{r}})}{|\mathbf{r}^3|} \quad (32)$$

for the flow field around a sphere with no-slip boundary conditions in the Stokes regime [71]. Here  $\mathbf{u}$  is the fluid velocity at infinity,  $\mathbf{r}$  is the position vector from the center of the colloid, and  $\hat{\mathbf{r}} = \mathbf{r}/|\mathbf{r}|$ . We assume that the flow field is  $\mathbf{u} = f/6\pi\eta R_H$  at infinity such that  $R_H$  is the only fit parameter in Eq. (32). For the two considered system sizes  $L = 80a$  and  $50a$ , we obtain the hydrodynamic radii  $R_H = 3.075a$  and  $3.25a$ , respectively, which are slightly smaller than the values extracted from the translational and rotational correlation functions. The simulation data agree well with the theoretical expression. In particular, the flow velocity in the colloid interior is very close to zero and the no-slip boundary condition is very well satisfied.

## VI. CONCLUSION

We have investigated the hydrodynamic properties of a colloid, which is modeled as a spherical shell of point particles immersed in a MPC fluid. We have analyzed the short-time MPC-collision-dominated regime and the long-time behavior. The simulation results can be well described by two analytical models: a hard-sphere neutrally buoyed colloid and a colloid comprised of mass points. In particular, we find a long-time tail of the translational velocity correlation function, which is solely determined by the fluid properties. Studies for various surfaces-particle densities suggest that approximately a single

surface point particle per collision cell provides excellent agreement with theoretical descriptions. For the colloid with radius  $R = 3a$ , this corresponds to the surface density  $\sigma a^2 \approx 0.53$ . Larger densities may give rise to additional inertia effects.

We have applied two strategies to extract a diffusion coefficient in the asymptotic limit of an infinitely large system. First, we performed simulations for various system sizes and extrapolated the hydrodynamic contribution of the diffusion coefficient to infinitely large systems. Second, we integrated the velocity autocorrelation function, where the long-time behavior is replaced by an analytical expression. Both procedures yield the same diffusion coefficient.

By comparing the correlation functions for translation and rotation motion of the discrete-point-particle model with those of a solid, neutrally buoyant colloid, we conclude that the discrete model describes the hydrodynamic properties of colloids surprisingly well. This is supported by the flow profile around such a sedimenting colloid, where we find essentially a zero fluid velocity inside the colloid and very good agreement with theoretical predictions of the flow velocities outside the colloid.

The simulations of the discrete-point-particle colloid have been performed with a non-angular-momentum-conserving MPC algorithm: the stochastic rotation algorithm [11]. In contrast, the simulations of the neutrally buoyant hard-sphere colloid have been performed with an angular-momentum-conserving MPC approach [32,48]. (For angular-momentum-conserving SRD simulations see Refs. [48,49].) The agreement between the simulation results for the velocity correlation functions (cf. Fig. 10) suggests that the lack or presence of angular momentum conservation has very little or no effect on the colloid dynamics for the no-slip boundary condition.

In summary, the discrete-particle model provides a valuable alternative to a solid colloid as far as hydrodynamic aspects are concerned, with considerably reduced numerical effort. This is particularly interesting for more complex structures such as coarse-grained protein models with mobile domains [78].

## ACKNOWLEDGMENTS

The authors thank M. Theers for helpful discussions. Financial support from the European Union through the FP7-Infrastructure project ESMI (Grant No. 262348) is gratefully acknowledged.

## APPENDIX A: VELOCITY CORRELATION FUNCTION

Here we calculate the colloid center-of-mass velocity autocorrelation function after one collision step. Thereby, we utilize the following relations.

(i) Since the dynamics of the colloid is force free between collisions,  $\hat{\mathbf{V}}(t) = \mathbf{V}(t-h)$ , i.e., the colloid center-of-mass velocity after a collision  $\mathbf{V}(t-h)$  is equal to that after the subsequent streaming step  $\hat{\mathbf{V}}(t)$ .

(ii) Both the colloid-surface particles and the MPC particles are in thermal equilibrium at any time. Hence,

$$\langle \mathbf{v}_i(t) \cdot \hat{\mathbf{V}}_k(t) \rangle = 0, \quad (\text{A1})$$

$$\langle \hat{\mathbf{V}}_j(t) \cdot \hat{\mathbf{V}}_k(t) \rangle = \frac{3k_B T}{M} \delta_{jk}. \quad (\text{A2})$$

The colloid center-of-mass VACF is

$$\begin{aligned}
 \langle \mathbf{V}(h) \cdot \mathbf{V}(0) \rangle &= \langle \mathbf{V}(h) \cdot \hat{\mathbf{V}}(h) \rangle \\
 &= \frac{1}{N_s^2} \sum_{i=1}^{N_s} \sum_{j=1}^{N_s} \langle \mathbf{V}_i(h) \cdot \hat{\mathbf{V}}_j(h) \rangle \\
 &= \langle \mathbf{V}(0)^2 \rangle + \frac{1}{N_s^2} \sum_{i=1}^{N_s} \sum_{j=1}^{N_s} \langle \{[\mathbf{R}(\alpha) - \mathbf{E}][\hat{\mathbf{V}}_i(h) - \mathbf{v}_{\text{c.m.}}(h)]\} \cdot \hat{\mathbf{V}}_j(h) \rangle, \tag{A3}
 \end{aligned}$$

with the collision rule (3) and  $\mathbf{v}_{\text{c.m.}}$  from Eq. (6). Averaging over the random orientation of the rotation axis and insertion of Eq. (A1) yields for the last term of Eq. (A3)

$$\frac{2}{3}[\cos(\alpha) - 1] \langle [\hat{\mathbf{V}}_i(h) - \mathbf{v}_{\text{c.m.}}(h)] \cdot \hat{\mathbf{V}}_j(h) \rangle = \frac{2}{3}[\cos(\alpha) - 1] \left[ \langle \hat{\mathbf{V}}_i(h) \cdot \hat{\mathbf{V}}_j(h) \rangle - \frac{\sum_{k=1}^{N_c^p} M \langle \hat{\mathbf{V}}_k(h) \cdot \hat{\mathbf{V}}_j(h) \rangle}{mN_c + MN_c^p} \right], \tag{A4}$$

where the sum with the index  $k$  runs over the colloid-surface particles in the collision cell of particle  $i$ . Utilization of Eq. (A2) finally gives

$$\langle \mathbf{V}(h) \cdot \mathbf{V}(0) \rangle = \frac{3k_B T}{MN_s} (1 - \mu), \tag{A5}$$

with

$$\mu = \frac{2}{3}(1 - \cos \alpha) \frac{m \langle N_c \rangle}{m \langle N_c \rangle + M \langle N_c^p \rangle}. \tag{A6}$$

The latter particularly applies for a single colloid-surface particle in a collision cell, i.e., for  $N_c^p = 1$ . Note that we assumed that every collision cell contains the same amount of fluid and colloid-surface particles in the derivation of Eq. (A5). In Eq. (A6) we replaced that number by the respective average number. To be more precise, the average in Eq. (A3) should also include an average over the respective particle numbers, which would be a Poisson distribution for the fluid particles [19]. During subsequent collisions, hydrodynamic correlations build up. However, if we neglect these correlations, i.e., assume that the molecular chaos assumption applies, the velocity correlation function after the time  $t$  is

$$\langle \mathbf{V}(t) \cdot \mathbf{V}(0) \rangle = \frac{3k_B T}{MN_s} (1 - \mu)^{t/h}. \tag{A7}$$

## APPENDIX B: HYDRODYNAMIC TENSOR

The solution for the fluid velocity field  $\mathbf{v}(\mathbf{k}, t)$  in Fourier space of the linearized Landau-Lifshitz Navier-Stokes

equations is given by

$$\mathbf{v}(\mathbf{k}, t) = \int \mathbf{Q}(\mathbf{k}, t - t') \mathbf{f}(t') dt', \tag{B1}$$

with the hydrodynamic tensor  $\mathbf{Q}(\mathbf{k}, t - t')$  and the volume force density  $\mathbf{f}(t)$  [13,70]. The tensor itself is composed of a transverse  $\mathbf{Q}^T$  and a longitudinal  $\mathbf{Q}^L$  part, where  $\mathbf{Q}(\mathbf{k}, t) = \mathbf{Q}^T(\mathbf{k}, t) + \mathbf{Q}^L(\mathbf{k}, t) = \mathbf{Q}^T(\mathbf{k}, t)(\mathbf{E} - \mathbf{P}) + \mathbf{Q}^L(\mathbf{k}, t)\mathbf{P}$ , with  $\mathbf{P}$  the projection operator with the components  $P_{\beta\beta'} = k_\beta k_{\beta'}/k^2$  and  $\mathbf{E}$  the unit tensor. Explicitly, the transverse part  $\mathbf{Q}^T$  is given by

$$\mathbf{Q}^T(\mathbf{k}, t) = \frac{1}{\rho} e^{-\nu k^2 t} \Theta(t), \tag{B2}$$

where  $\Theta(t)$  is the Heaviside function,  $\nu = \eta/\rho$  denotes the kinematic viscosity, and  $\rho$  is the mass density. For the MPC fluid, the viscosity  $\eta = \eta^k + \eta^c$  is composed of a kinetic  $\eta^k$  and collisional  $\eta^c$  contribution [22]. The longitudinal part  $\mathbf{Q}^L$  reads

$$\mathbf{Q}^L(\mathbf{k}, t) = \frac{1}{\rho} e^{-k^2 \tilde{\nu} t/2} \left[ \cos(\Omega t) - \sqrt{\frac{k^2 \tilde{\nu}^2}{4c^2 - k^2 \tilde{\nu}^2}} \sin(\Omega t) \right] \Theta(t) \tag{B3}$$

for  $4c^2/k^2 \tilde{\nu}^2 > 1$ , where  $\Omega = k^2 \tilde{\nu} \sqrt{4c^2/k^2 \tilde{\nu}^2 - 1}/2$ ,  $\tilde{\nu} = \tilde{\eta}/\rho = (\eta + \eta^k/3)/\rho$ , and

$$\mathbf{Q}^L(\mathbf{k}, t) = \frac{1}{\rho} e^{-k^2 \tilde{\nu} t/2} \left[ \cosh(\Lambda t) - \sqrt{\frac{k^2 \tilde{\nu}^2}{k^2 \tilde{\nu}^2 - 4c^2}} \sinh(\Lambda t) \right] \times \Theta(t) \tag{B4}$$

for  $4c^2/k^2 \tilde{\nu}^2 < 1$ , where  $\Lambda = k^2 \tilde{\nu} \sqrt{1 - 4c^2/k^2 \tilde{\nu}^2}/2$  [13].

- [1] *Coarse-Graining of Condensed Phase and Biomolecular Systems*, edited by G. A. Voth (CRC, Boca Raton, 2008).  
 [2] D. Reith, M. Pütz, and F. Müller-Plathe, *J. Comput. Chem.* **24**, 1624 (2003).  
 [3] A. P. Lyubartsev and A. Laaksonen, *Phys. Rev. E* **52**, 3730 (1995).

- [4] F. Ercolessi and J. B. Adams, *Europhys. Lett.* **26**, 583 (1994).  
 [5] S. Izvekov and G. A. Voth, *J. Chem. Phys.* **123**, 134105 (2005).  
 [6] W. G. Noid, J. W. Chu, G. S. Ayton, and G. A. Voth, *J. Phys. Chem. B* **111**, 4116 (2007).  
 [7] S. J. Marrink, A. H. de Vries, and A. E. Mark, *J. Phys. Chem. B* **108**, 750 (2004).

- [8] G. R. McNamara and G. Zanetti, *Phys. Rev. Lett.* **61**, 2332 (1988).
- [9] P. J. Hoogerbrugge and J. M. V. A. Koelman, *Europhys. Lett.* **19**, 155 (1992).
- [10] A. Malevanets and R. Kapral, *J. Chem. Phys.* **110**, 8605 (1999).
- [11] G. Gompper, T. Ihle, D. M. Kroll, and R. G. Winkler, *Adv. Polym. Sci.* **221**, 1 (2009).
- [12] R. Kapral, *Adv. Chem. Phys.* **140**, 89 (2008).
- [13] C.-C. Huang, G. Gompper, and R. G. Winkler, *Phys. Rev. E* **86**, 056711 (2012).
- [14] A. Malevanets and J. M. Yeomans, *Europhys. Lett.* **52**, 231 (2000).
- [15] A. Malevanets and R. Kapral, *J. Chem. Phys.* **112**, 7260 (2000).
- [16] M. Ripoll, K. Mussawisade, R. G. Winkler, and G. Gompper, *Europhys. Lett.* **68**, 106 (2004).
- [17] T. Ihle and D. M. Kroll, *Phys. Rev. E* **63**, 020201(R) (2001).
- [18] T. Ihle and D. M. Kroll, *Phys. Rev. E* **67**, 066706 (2003).
- [19] N. Kikuchi, C. M. Pooley, J. F. Ryder, and J. M. Yeomans, *J. Chem. Phys.* **119**, 6388 (2003).
- [20] C. M. Pooley and J. M. Yeomans, *J. Phys. Chem. B* **109**, 6505 (2005).
- [21] A. Lamura, G. Gompper, T. Ihle, and D. M. Kroll, *Europhys. Lett.* **56**, 319 (2001).
- [22] R. G. Winkler and C.-C. Huang, *J. Chem. Phys.* **130**, 074907 (2009).
- [23] K. Mussawisade, M. Ripoll, R. G. Winkler, and G. Gompper, *J. Chem. Phys.* **123**, 144905 (2005).
- [24] C.-C. Huang, R. G. Winkler, G. Sutmann, and G. Gompper, *Macromolecules* **43**, 10107 (2010).
- [25] M. A. Webster and J. M. Yeomans, *J. Chem. Phys.* **122**, 164903 (2005).
- [26] J. F. Ryder and J. M. Yeomans, *J. Chem. Phys.* **125**, 194906 (2006).
- [27] M. Ripoll, R. G. Winkler, and G. Gompper, *Phys. Rev. Lett.* **96**, 188302 (2006).
- [28] L. Cannavacciuolo, R. G. Winkler, and G. Gompper, *Europhys. Lett.* **83**, 34007 (2008).
- [29] S. H. Lee and R. Kapral, *J. Chem. Phys.* **121**, 11163 (2004).
- [30] M. Hecht, J. Harting, T. Ihle, and H. J. Herrmann, *Phys. Rev. E* **72**, 011408 (2005).
- [31] J. T. Padding and A. A. Louis, *Phys. Rev. E* **74**, 031402 (2006).
- [32] I. O. Götzke, H. Noguchi, and G. Gompper, *Phys. Rev. E* **76**, 046705 (2007).
- [33] M. K. Petersen, J. B. Lechan, S. J. Plimpton, G. S. Grest, P. J. in't Veld, and P. R. Schunk, *J. Chem. Phys.* **132**, 174106 (2010).
- [34] J. K. Whitmer and E. Luijten, *J. Phys.: Condens. Matter* **22**, 104106 (2010).
- [35] T. Franosch, M. Grimm, M. Belushkin, F. M. Mor, G. Foffi, L. Forró, and S. Jeney, *Nature (London)* **478**, 85 (2011).
- [36] M. Belushkin, R. G. Winkler, and G. Foffi, *J. Phys. Chem. B* **115**, 14263 (2011).
- [37] J. Schofield, P. Inder, and R. Kapral, *J. Chem. Phys.* **136**, 205101 (2012).
- [38] H. Noguchi and G. Gompper, *Phys. Rev. Lett.* **93**, 258102 (2004).
- [39] H. Noguchi and G. Gompper, *Proc. Natl. Acad. Sci. USA* **102**, 14159 (2005).
- [40] J. L. Mcwirthner, H. Noguchi, and G. Gompper, *Proc. Natl. Acad. Sci. USA* **106**, 6039 (2009).
- [41] V. Lobaskin and B. Dünweg, *New J. Phys.* **6**, 54 (2004).
- [42] S. C. Glotzer and M. J. Solomon, *Nat. Mater.* **6**, 557 (2007).
- [43] J. de Graaf, R. van Roij, and M. Dijkstra, *Phys. Rev. Lett.* **107**, 155501 (2011).
- [44] P. F. Damasceno, M. Engel, and S. C. Glotzer, *Science* **337**, 453 (2012).
- [45] M. P. Allen and D. J. Tildesley, *Computer Simulation of Liquids* (Clarendon, Oxford, 1987).
- [46] W. C. Swope, H. C. Andersen, P. H. Berens, and K. R. Wilson, *J. Chem. Phys.* **76**, 637 (1982).
- [47] E. Allahyarov and G. Gompper, *Phys. Rev. E* **66**, 036702 (2002).
- [48] H. Noguchi and G. Gompper, *Phys. Rev. E* **78**, 016706 (2008).
- [49] M. Theers and R. G. Winkler, *Soft Matter* **10**, 5894 (2014).
- [50] C.-C. Huang, A. Chatterji, G. Sutmann, G. Gompper, and R. G. Winkler, *J. Comput. Phys.* **229**, 168 (2010).
- [51] M. Yang, A. Wysocki, and M. Ripoll, *Soft Matter* **10**, 6208 (2014).
- [52] I. O. Götzke and G. Gompper, *Phys. Rev. E* **82**, 041921 (2010).
- [53] M. Ripoll, K. Mussawisade, R. G. Winkler, and G. Gompper, *Phys. Rev. E* **72**, 016701 (2005).
- [54] E. Westphal, S. Singh, C.-C. Huang, G. Gompper, and R. Winkler, *Comput. Phys. Commun.* **185**, 495 (2014).
- [55] M. Belushkin, R. G. Winkler, and G. Foffi, *Soft Matter* **8**, 9886 (2012).
- [56] E. Tüzel, T. Ihle, and D. M. Kroll, *Phys. Rev. E* **74**, 056702 (2006).
- [57] S. Chapman and T. G. Cowling, *The Mathematical Theory of Non-Uniform Gases* (Cambridge University Press, Cambridge, 1990).
- [58] G. Subramanian and H. T. Davis, *Phys. Rev. A* **11**, 1430 (1975).
- [59] J. T. Hynes, *Annu. Rev. Phys. Chem.* **28**, 301 (1977).
- [60] C. S. Pangali and B. J. Berne, *J. Chem. Phys.* **67**, 4571 (1977).
- [61] J. T. Padding, A. Wysocki, H. Löwen, and A. A. Louis, *J. Phys.: Condens. Matter* **17**, S3393 (2005).
- [62] J.-P. Hansen and I. R. McDonald, *Theory of Simple Liquids* (Academic, London, 1986).
- [63] E. H. Haug and A. Martin-Löf, *J. Stat. Phys.* **7**, 259 (1973).
- [64] D. Bedeaux and P. Mazur, *Physica* **76**, 247 (1974).
- [65] E. J. Hinch, *J. Fluid Mech.* **72**, 499 (1975).
- [66] H. Metiu, D. W. Oxtoby, and K. F. Freed, *Phys. Rev. A* **15**, 361 (1977).
- [67] B. U. Felderhof, *J. Chem. Phys.* **123**, 044902 (2005).
- [68] J. K. G. Dhont, *An Introduction to Dynamics of Colloids* (Elsevier, Amsterdam, 1996).
- [69] A. Erbas, R. Podgornik, and R. R. Netz, *Eur. Phys. J. E* **32**, 147 (2010).
- [70] C.-C. Huang, G. Gompper, and R. G. Winkler, *J. Chem. Phys.* **138**, 144902 (2013).
- [71] L. D. Landau and E. M. Lifshitz, *Fluid Mechanics* (Pergamon, Oxford, 1987).
- [72] J. A. Montgomery and B. J. Berne, *J. Chem. Phys.* **67**, 4580 (1977).
- [73] J. A. Montgomery and B. J. Berne, *J. Chem. Phys.* **66**, 2770 (1977).
- [74] I. Yeh and G. Hummer, *J. Phys. Chem. B* **108**, 15873 (2004).

- [75] A. J. C. Ladd, R. Kekre, and J. E. Butler, *Phys. Rev. E* **80**, 036704 (2009).
- [76] S. P. Singh, C.-C. Huang, E. Westphal, G. Gompper, and R. G. Winkler, *J. Chem. Phys.* **141**, 084901 (2014).
- [77] S. Frank and R. G. Winkler, *Europhys. Lett.* **83**, 38004 (2008).
- [78] L. Hong, M. A. Sharp, S. Pobleto, R. Biehl, M. Zamponi, N. Szekely, M.-S. Appavou, R. G. Winkler, R. Nauss, A. Johs, J. M. Parks, Z. Yi, X. Cheng, L. Liang, M. Ohl, S. M. Miller, D. Richter, G. Gompper, and J. C. Smith, *Biophys. J.* **107**, 393 (2014).